Aerodynamics of a Radial Jet from a Tube Breach in a Shell-and-Tube Heat Exchanger

F.J. Sánchez-Velasco, C. López del Prá, Luis E. Herranz

Nuclear Safety Research Unit, CIEMAT Research Center, Madrid, Spain, franciscoj.sanchez@ciemat.es

Abstract This paper summarizes the major insights gained into the aerodynamics of a radial jet entering a tube bundle from a guillotine tube breach. This scenario is highly relevant in nuclear safety since it determines the potential retention of radioactive particles during risk-dominant sequences, the so called Steam Generator Tube Rupture (SGTR) sequences. A scaled-down mock-up with representative dimensions of a real steam generator was used in two different configurations of the experimental rig. Two dimensional (2D) PIV technique was used to characterize the flow field in the space between the breach and the neighbor tubes in the range investigated (100-250 kg/h i.e. Re_D=1-2.7·10^5). The results are reported and discussed in terms of velocity, turbulent intensity, jet trajectory and spreading rate, for both the "in-bundle" jet and the radial free jet. The presence of tubes was observed to have two major effects: a distortion of the jet shape and an increase of the maximum jet velocity and turbulence near the breach. Enhancing factors ranged from 1.6 to 3.5 for velocity and form 2 to 3.2 for turbulent intensity. The increase of the inlet gas mass flow rate increases the Tu and the maximum velocity reached. Data from this research is being used to validate 3D CFD simulations.

Nomenclature

Δt	pulse lapse
Δx	spatial displacement
$\Delta x'$	pixel displacement
AMMD	Aerodynamic mass median diameter
b	spreading rate defined as the value of eta where $U=0.5U_{max}$
CAHT	Ciemat Artist hydrodynamics tests
eta	coordinate normal to the jet axis
GSD	geometric standard deviation
OPC	optical particle counter
p	pitch minimum distance between the surface of neighbor tubes
P	pressure sensor
PDF	probability density function
PECA	Platform for experimental characterization of aerosols
Q	mass flow rate sensor
r	radial distance to the axis of the broken tube
Re_D. $=U_o \cdot D_{Tube}/\nu$	tube Reynolds number
$Re_p= U_o \cdot d_{particle}/\nu$	particle Reynolds number
Re_H. $=U_o \cdot H/\nu$	impinging jets Reynolds number
$Stk = C_c \frac{\rho_p \cdot d_p^2 \cdot v_{gas}}{18 \cdot \mu_{gas} \cdot d_T}$	Stokes Number
Tu	turbulence intensity level based on the local velocity at each point: $100 \cdot u_{rms}/U_{local}$
U, V	velocity
y	axial distance to the breach center

1. Introduction

Pressurized nuclear power reactors rely on vertical shell and tube heat exchangers to produce the steam that eventually expands through the turbine of a Rankine cycle. During the plant operation a variety of phenomena (i.e., stress corrosion cracking, erosion-corrosion, high-cycle fatigue, etc.) may degrade the boundary between the primary and the secondary side until resulting in a tube rupture. Under the very unlikely circumstances of a reactor core melting, such a failure could become a direct leak of radioactive particles to the environment. This scenario, generally called Steam Generator Tube Rupture (SGTR), is of an outstanding importance in nuclear safety.

The steam generator (SG) is a complex structure housing various components and around 4000 U-inverted tubes. Under normal working conditions its secondary side is flooded with water to generate steam. Under accident conditions, however, the tube breach could be over the water level and radioactive particles would enter a “dry” secondary side carried by a high-velocity gas flow.

A sound and comprehensive database on the aerosol retention in the secondary side of a vertical SG is being set up within the international ARTIST project (Güntay et al., 2004). Even though these new results are not available yet, some bench-scale data were already obtained within the EU-SGTR project (Auvinen, et al., 2005). Experiments showed that, under dry conditions, a guillotine-type breach would result in a gas radial jet emerging from the primary circuit into the secondary one. Particles carried by the gas would deposit on the tubes near the breach primarily by inertial impaction and turbulent deposition (Herranz et al., 2006). Both depletion mechanisms are extremely dependent on the flow field across the tube bundle. Therefore, the aerodynamic characterization of the flow field in the scenario is of major importance for the complete understanding and accurate modeling of these mechanisms.

This paper summarizes the major insights gained from 2D PIV measurements into the aerodynamics of a radial jet entering the secondary side of the steam generator from a guillotine tube breach. In particular, the effect of the presence of tubes and the influence of the gas mass flow rate on the jet behavior have been explored. Given the importance of tubes around the breach in aerosol retention, specific attention has been paid to the jet behavior in the space between the broken tube and the first neighbor tubes. Shortcomings of the PIV technique applicability in this scenario and the ways to overcome them are also discussed in this paper.

2. Aerodynamic background

The aerodynamic scenario outlined above is complex and specific. No previous investigations have been found in the open literature. However, investigations carried out by other authors on scenarios with some similarities can provide meaningful highlights for the present research. In particular, a survey has been conducted on:

- Turbulent radial free jets (Abramovich 1963; Schwarz, 1963; Heskestad, 1966; Rajaratman, 1976; Witze and Dwyer 1976)
- Plane jets in cross-flow (Girshovich 1966; Choi and Wood 1966)
- Impinging jets on cylinders (Schuh and Persson 1964; Cornaro et al. 1999; Sparrow et al. 1980)
- Cross-flow streams in a tube bundle (Incropera and Dewitt, 1996)
- Axial flow streams in a tube bundle (Seale (1981), Hooper (1980), Rowe et al. (1974)).

The most significant results from these studies can be summarized as follows:

- In radial free jets, the maximum velocity in the fully developed region is inversely proportional to the distance from the inlet point. The spreading rate, however, is directly proportional (Schwarz, 1963).

- In radial jets generated from the impingement of two opposing round free jets, Witze and Dwyer (1976) found that a constrained radial jet (Re_H~$2\cdot10^3$ and H/D=0.005-0.06) spreads at the same rate as does the plane jet, while the free impinged radial jet (Re_H~$2\cdot10^5$ and H/D=20-42) spreads at a rate more than three times as fast.

- In cross-flow plane jets of incompressible fluids, Choi and Wood (1966) found that for different initial jet angles (9º, 17º, 25º and 45º), the growth rate of the jets on either side of the jet axis was found to be unequal and the growth of the total width with respect to the jet axis coordinate was not linear. For initial jet angles smaller than 25º the trajectories of the jet axis were well correlated by the system $x/(\alpha^2\delta_o)$ vs $y/(\alpha^2\delta_o)$, where α is the jet to free stream velocity ratio (2.6-9.0) and δ_o is the thickness of the jet at the nozzle.

- In free jets impinging on cylinders, Schuh and Persson (1964) found that for a specific ratio of jet-to-cylinder diameter and distance to the nozzle, transport phenomena were considerably enhanced with respect to parallel flow over the cylinder surface at Re_D.=2-$6\cdot10^4$. This result is explained by the ability of thin jets to adhere to curved surfaces (Coanda effect) and the high intensity of turbulence in a jet.

3. Experimental set-up

The experimental campaign was carried out in two phases. The first one was devoted to study aerodynamics of a free radial jet from a broken tube, and it was carried out within the vessel of the so called PECA facility (Fig. 1). The second one was focused on investigating “in-bundle” jet behavior, and it was conducted within a methacrylate structure hereafter named CAHT (Figs. 2-4). Both set-ups shared the main experimental systems: air supply system, aerosol generator, steam generator mock-up and data acquisition system. A total of four tests at different gas flow rates (107 kg/h, 139 kg/h, 204 kg/h and 254 kg/h) were executed in each facility. Some of the experiments were carried out more than once to confirm reproducibility. No thermal and steam concentration gradients were predicted in the scenarios (Güntay et al., 2002), so that air was used and room temperature and pressure were set in all the tests.

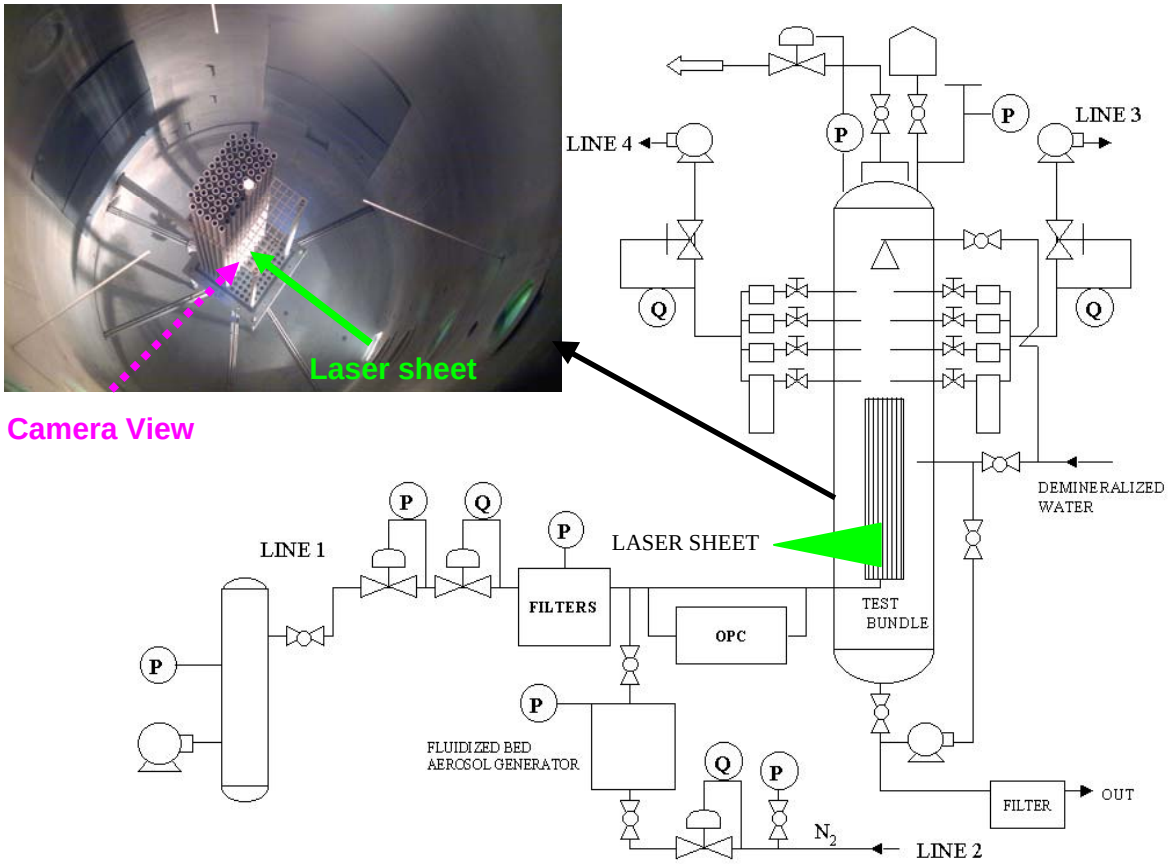

Fig. 1. Scheme of the PECA facility and bundle configuration in the vessel

Table 1 compares the main aerodynamic-related variables and non-dimensional numbers characterizing the SGTR sequences to those achieved in the experimental facility.

Table 1. Variables and non-dimensional numbers characterizing SGTR scenarios

	D (m)	U_{gas} (m/s)	Re_D	Stk	Re_p^2 / Stk
SGTR	10^{-2}	10 – 300	$10^4 – 10^6$	$10^{-2} – 10$	10^2 - 10^3
CAHT-PECA	10^{-2}	10 – 200	$10^4 – 10^5$	$10^{-2} – 10$	10^2 - 10^3

The mock-up is a scaled-down assembly simulating the break stage of the secondary side of the SG. It consists of a square array of 11x11 tubes (330 x 330 x 1000 mm), supported by an upper and a lower plate. This limited size was backed by CFD analyses (Herranz el al., 2005). The dimensions of the tubes and the support plate are identical to those used in a stage of real SG of a nuclear power plant (Güntay et al, 2004). The tubes are D=19.05 mm in diameter with a pitch-to-diameter ratio in the bundle of p/d=0.4. The break height is H=0.24·D and it is placed in the central tube at 0.24 m from the base. The flow is injected into the broken tube through the base. Since the end of the tube is closed, the flow is forced to exit through the breach and to expand across the bundle.

Fig. 2. CAHT configuration

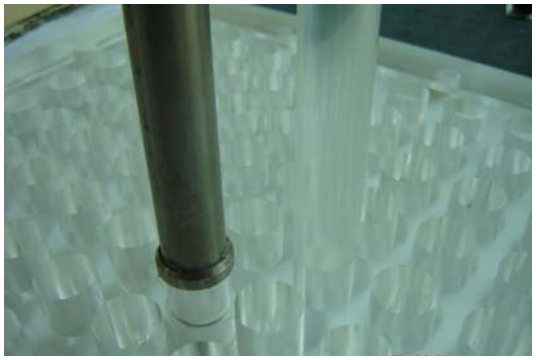

Fig. 3. Transparent tubes

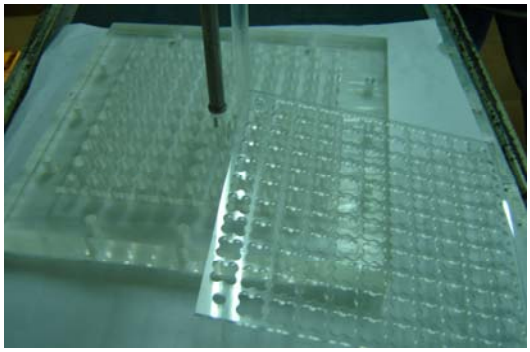

Fig. 4. Methacrylate base and support plate

The first configuration made it feasible to avoid any bounding constraint, whereas the second one improved considerably the optical access. Some tubes were substituted by transparent ones to reduce the laser sheet reflection on their surface and to improve the imaging closer to it. Figs. 1 and 2 indicate the laser–camera arrangement in each set-up. As shown, the laser sheet was generated from a side of the PECA vessel and contained the axis of the broken tube, whereas it entered the CAHT frame from the bottom and extended upwards containing also the axis of the broken tube.

A standard 1660 x 1200 pixels PIV cross-correlation CCD camera, a pulsed Nd:Yag laser and three different lenses (28mm, 135mm and 300mm F2.8) were used to record images. TiO_2 was used as seeding material. The aerosol generator is based on fluidized bed technology and permits the injection of up to 15 kg/h N_2-seed-flow at high pressure. Once the steady state of each test is reached, 310 pairs of images were taken at 15Hz.

4. Results and discussion

The results from the experimental campaign provided data concerning free radial jets and jets in tube bundle. The radial free jet was characterized and adopted as a reference to assess the effect of the tubes on the jet behavior. The main kinematic variables derived from the PIV measurements were: mean velocity field, turbulence quantities, jet center line trajectory and jet spreading rate. This investigation was focused on the space between the broken tube and its closest neighbor.

The applicability of the PIV technique to this scenario suffered from several shortcomings due to

the light scattering of the laser sheet onto the tubes surfaces. This scattering increases the background intensity on the images and reduces drastically the quality of the cross correlation. As a result, no data can be recorded near the tubes surfaces. Several methods were tested to overcome this problem. The most fruitful was the use of transparent material for the tubes, so that the laser sheet partially goes through the surface and the light scattering is partially reduced.

4.1 The radial free jet

The radial free jet near the breach was characterized using the PECA configuration (Fig. 1). Velocity measurements were obtained in a vertical plane extended radially from the broken tube axis (60x70 mm). Fig. 7 illustrates the particular case of 107 kg/h. Two general observations can be made from the results:

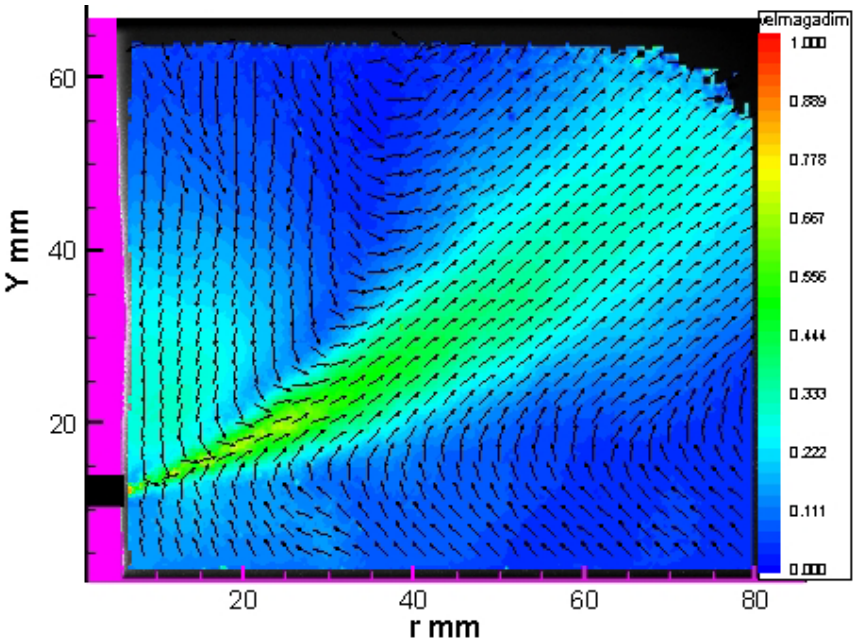

Fig. 7. Normalized mean velocity field for 107 kg/h free radial jet

- The jet enters the domain with an initial deflection angle and bends upwards as an oblique axi-symmetric jet. This is a consequence of the location of gas exit at the top of the vessel, which drags the jet vertically.

- The entrainment of surrounding gas caused by the jet is not symmetric. The parabolic shape of the jet enhances gas suction at the concave side with respect to the convex one.

The jet trajectory can be well fitted to a parabolic curve as shown in Fig. 8. The initial jet angle, jet trajectory, and jet penetration in the region explored remain nearly invariable when the inlet mass flow rate was varied.

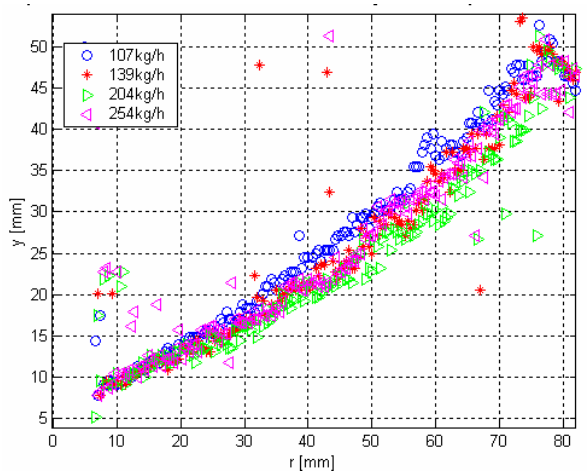

Fig. 8. Jet trajectory with the radial distance to the breach

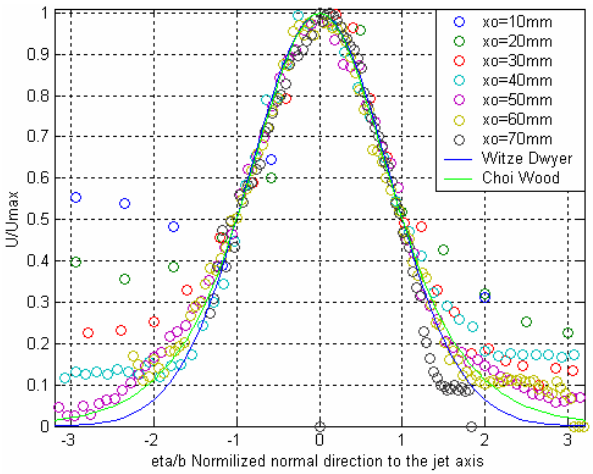

Fig. 9. Velocity profiles measured along the jet center line for different radial distances to the breach. 107 kg/h case

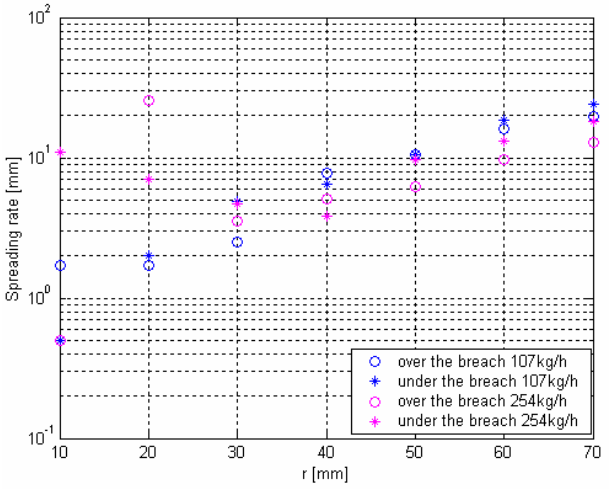

Fig. 10. Spreading rate evolution with the radial distance to the breach

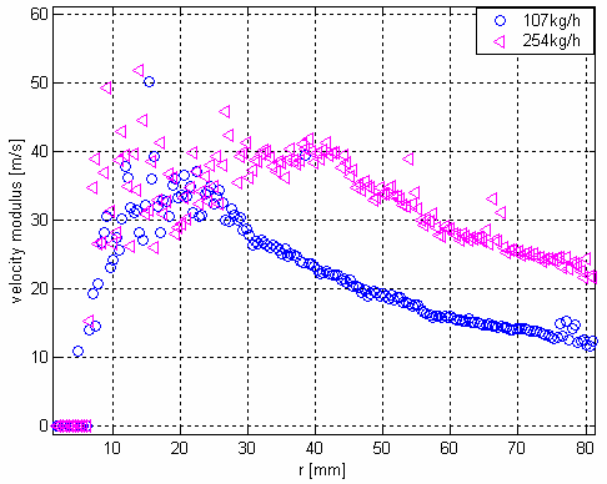

Fig. 11. Maximum jet velocity evolution with the radial distance to the breach

Fig. 9 shows the jet dimensionless velocity profiles over the normal direction to the jet axis at several radial distances for the case 107 kg/h. As in Fig. 7, two regions can be differentiated: the "entry region" and the "fully-developed region". In the former, velocity profiles are still under development and gas entrainment from the upper region affects them noticeably. As a result, profiles are asymmetric: the jet core shows a normal distribution, whereas at the jet rim relative velocities at the upper side are higher than those at the lower one. In the latter, the gas suction effect, if any, is negligible and the dimensionless velocity profile follows a Gaussian distribution. As compared to other jet topologies, like non-deflected radial jet profiles (Witze and Dwyer, 1976) and oblique cross flowing jet profiles (Choi and Wood, 1966), data show a great consistency in the fully developed region. Thus, differences in jet behavior from topology vanish at a certain distance from the entry point.

Gas mass flow rate affects velocity profiles in a different way depending of the jet region. Asymmetry of the "entry region" is exacerbated as gas mass flow rate increases, whereas the "fully-developed region" hardly changes. This observation is further illustrated through the spreading rate

and maximum velocity evolutions (Fig. 10 and 11, respectively):

- Spreading rates are notably different at the upper and the lower sides of the jet core in the "entry region": the higher the flow rates, the more noticeable the discrepancies. In the "fully-developed" region, however, upper and lower differences disappear and all the flow rates collapse within a band well within the uncertainty range.

- The maximum jet velocity accelerates until reaching its maximum value in the "entry region", and then it decreases smoothly. The radial location of the maximum moves away from the breach as gas flow rate increases. The effect of gas suction causes a large scattering of data in the entry region (this being even enhanced at high flow rates).

4.2 Jet in tube bundle

Jets expanding in a tube bundle were investigated using the CAHT configuration (Fig. 2).

Fig. 12 shows the free and in-bundle jet velocity fields obtained for 203.6 kg/h and 254.3 kg/h in the same radial region. It is worth to highlight that TiO_2 particles accumulated at neighbor tubes surface area facing the breach due to jet impingement. Such a deposit did affect the results summarized below:

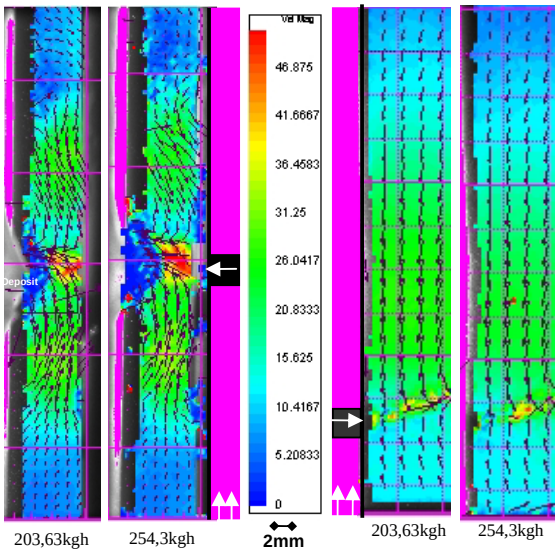

Fig. 12. Mean velocity field near the breach for the jet in tube bundle and for free jet

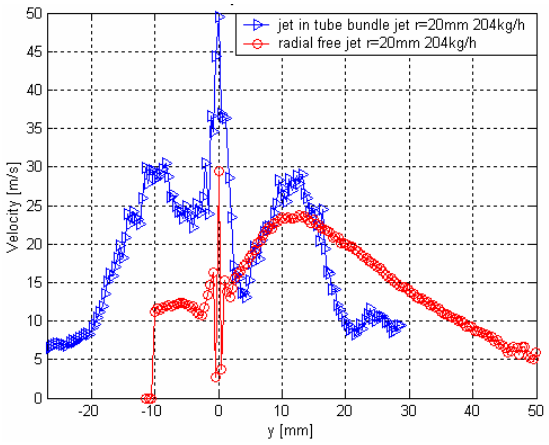

Fig. 13. Vertical profiles for the velocity modulus near the breach for the jet in tube bundle and for free jet

- The jet shape is drastically distorted with respect to the free jet one. The presence of tubes enhances the gas entrainment over and below the breach. This effect is especially important below the breach, where the velocity field increases in magnitude considerably (by a factor around 2). Fig. 13 shows the velocity profiles found at the breach exit for the jet with and without tubes. In the presence of tubes, the profiles show a quasi-symmetric shape with two relative maximums related to the entrainment of flow.

- The magnitude of the jet velocity is increased with respect to the free jet one (by a factor

between 1.6 and 3.5). The tube bank reduces the cross section, so that for the same flow rate (assuming that compressible effects are small enough) a higher velocity is reached.

- The tubes decrease drastically the jet penetration. The impingement of the jet on the tube surface splits the jet that flows around and upwards over the tube surface. This surface-jet interaction causes a sharp reduction of jet radial momentum. This is consistent with the Coanda effect that enhances the adhesion of jets to curved surfaces and promotes the bending of the jet trajectory (Schuh and Person, 1964).

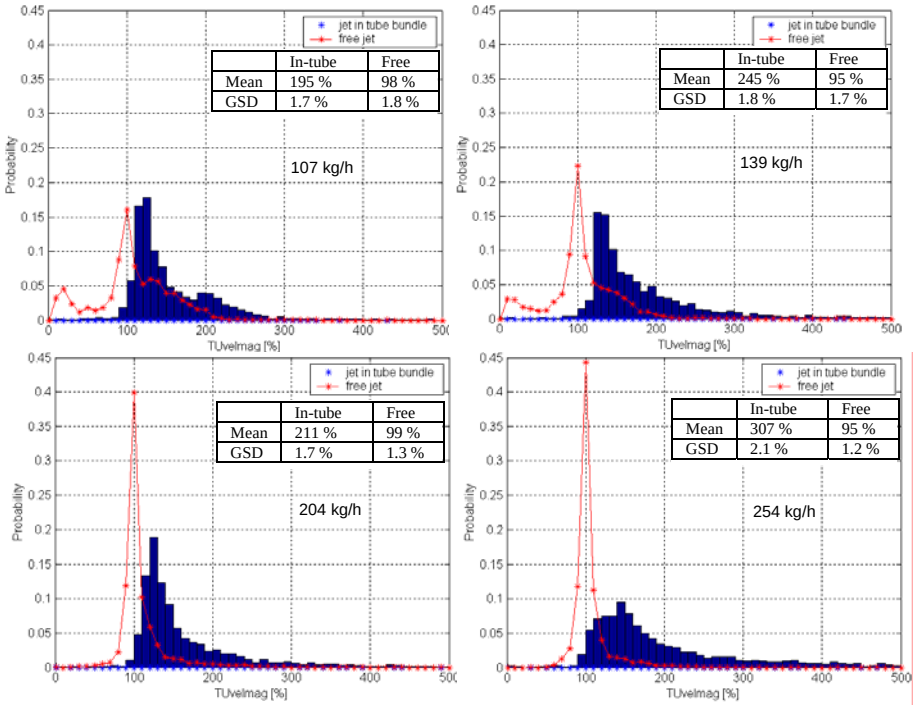

Fig. 14. Tu PDFs comparison for different mass flow rates for jet in tube bundle and free jet

- Turbulence intensity is also enhanced with respect to the free jet. Fig. 14 shows a comparison of the Tu PDFs. “In-bundle” jets follow a log-normal distribution where the mean and the GSD increase when the gas mass flow rate increases. However, the free jet distribution tends to adopt a Gaussian shape when increasing the inlet mass flow rate. Its mean remains constant (~100%) and the GSD decreases when the inlet mass flow rate increases. The presence of tubes seems to enhance two or three times the mean value of the turbulence in the area.

5. Uncertainty analysis

A total of 310 pairs of images were acquired during each test. According to Lourenço (1982) this sampling should yield an uncertainty associated to the turbulence nature of the flow of around 5% with a 95% confidence.

Regarding post-processing, a code to estimate PIV results uncertainty has been developed based on ISO Norm (1995). By using error propagation theory the uncertainty on the mean velocity field can be calculated as:

$$\delta V = \sqrt{\left(\frac{1}{M\Delta t}\delta\Delta x'\right)^2 + \left(-\frac{\Delta x'}{M^2\Delta t}\delta M\right)^2 + \left(-\frac{\Delta x'}{M\Delta t^2}\delta\Delta t\right)^2} \quad (1)$$

where

$$\Delta x' = M \cdot \Delta x \quad (2)$$

$$V = \frac{\Delta x'}{M \cdot \Delta t} \quad (3)$$

being M the magnification factor relating the real physical space (Δx) and the camera domain (Δx'). Table 2 shows the order of magnitude of the different uncertainty sources of variables in Eq. 4.

Table 2. Uncertainty source terms estimations

Source term	Estimation	Comments
Pulse separation	$\delta\Delta t = 0.1\mu s$	Obtained from hardware settings from TSI (1997)
Magnification factor M	$\delta M = 0.1 pixels/mm$	Calculated from the calibration process
Pixel displacement	$\delta\Delta x' = 0.1 pixels$	Depends on the processing algorithm. Order of magnitude estimated from Scarano and Riethmuller (2000)

The estimation of the magnification uncertainty (i.e. the quality of the spatial calibration) rose as the main factor affecting the final velocity uncertainty.
From all the above considerations, uncertainty in the PIV measurements of the mean velocity field has been estimated to be lower than 16% within a 95% of confidence level.

6. Final remarks and future work

A thorough characterization of the gas flow coming out from a broken tube under SGTR conditions has been carried out with 2D-PIV. By optimizing the experimental configuration and optical access, PIV provided data on aerodynamic variables relevant for radioactive particle retention in a challenging nuclear safety scenario. These data will be used to benchmark and validate CFD codes.

This investigation has demonstrated that the presence of tubes affects drastically the jet behavior. The jet tends to stick neighbor tube surfaces. As a result, jet penetration is attenuated, whereas upwards motion is fostered. Given the high level of turbulence measured in the presence of tubes, this jet bending means that particles would deposit on these first neighbor surfaces by turbulent mechanisms. In addition, the high velocities reached in the initial cross-flow orientation of the jet, make particles accumulate on neighbor surfaces facing the breach.

There are evidences that an increase of gas mass flow rates could enhance particle deposition by turbulent and inertial mechanisms. However, such an effect should be further investigated. In addition, more experiments are foreseen to extend the domain of this research to regions farther than the first neighbor tubes and to study how breach type could affect the jet aerodynamics.

7. Acknowledgements

The authors wish to thank the Spanish Nuclear Safety Council for their financial support to participate in the international ARTIST project.

8. References

Abramovich GN (1963) The theory of turbulent jets. Massachusetts: MIT Press

Auvinen A, Jokiniemia JK, Lähde A, Routamo T, Lundström P, Tuomistob H, Dienstbierc J, Güntay S, Suckow S, Dehbi A, Slootmane M, Herranz L, Peyres V, Polo J (2005) Steam generator tube rupture (SGTR) scenarios. Nucl Eng Des 235:457-472

Choi Y, Wood IR, (1966) Momentum diffusion from a two-dimensional jet. Report no 90, Water Research Laboratory. University of New South Wales, Australia

Cornaro C, Fleischer AS, Goldstein RJ (1999) Flow visualization of a round jet impinging on cylindrical surfaces. Exp Thermal Fluid Sci 6: 66-78

Girshovich TA (1966) Theoretical and experimental study of a plane turbulent jet in a cross-flow. Fluid Dyn 9:84-86

Güntay S, Dehbi A, Suckow D, Birchley J (2002) ARTIST: an international project investigating aerosol retention in a ruptured steam generator. Int congress on advanced nuclear power plants ICAPP'02, June 9-13, Hollywood, Florida

Güntay S, Suckow D, Dehbi A, Kapulla R (2004) ARTIST: introduction and first results. Nucl Eng Des 231:109-120

Herranz L, Del Prá CL, Velasco FJS, Muñoz-Cobo JL, Escrivá A (2005) Insights into aerosol depletion from a high velocity flow across a tube bank: a key scenario for nuclear safety. Proc of 6th World conf on experimental heat transfer, fluid mechanics and thermodynamics. April 17-21, Miyagi, Japan

Herranz L, Sánchez-Velasco FJ, Del Prá CL (2006) Aerosol retention near the tube breach during steam generator tube rupture sequences. Nucl Technol 154:85-94

Heskestad G (1966) Hot-wire measurements in a radial turbulent jet. Trans ASME J Appl Mech 417-424

Hooper JD (1980) Nucl Eng Des 60:365

Incropera FP and Dewitt DP (1996) Introduction to heat transfer. 3rd ed, USA: Willey Press

ISO NORM (1995) Guide to expression of uncertainty in measurement. Corrected and Reprinted. ISBN 92-67-10188-9. International Organization for Standardization, Geneva, Switzerland

Lourenço (1982) PhD Thesis, Von Karman Institute, Belgium

TSI Corporate (1997) PIV hardware operation's manual. P/N 1990831, St Paul, Minnesota, USA

Rajaratman N (1976) Turbulent Jets. Amsterdam: Elsevier Scientific Publishing Company

Rowe DS, Johnson BM, Knudsen JG (1974) Int J Heat Mass Transfer 17:407

Scarano F, Riethmuller ML (2000) Advances in iterative multigrid PIV image processing. Exp Fluids 29:S51-S60

Schuh H, Persson B (1964) Heat transfer on circular cylinders exposed to free-jet flow. Int. J. Heat Mass Transfer 7:1257-1271

Schwarz WH (1963) The radial free jet. Chem Eng Sci 18:779-786

Seale WJ (1982) Measurements and predictions of fully developed turbulent flow in a simulated rod bundle. J Fluid Mech 123:99-423

Sparrow EM, Lovell BJ (1980) Heat transfer characteristics of an obliquely impinging circular jet. J Heat Transfer 102:202-209

Witze PO, Dwyer HA (1976) The turbulent radial jet. J Fluid Mech 75:401-417